PCCP

Accepted Manuscript

ROYAL SOCIETY OF CHEMISTRY

www.rsc.org/pccp

Ultra-wide bandwidth with enhanced microwave absorption of electroless Ni-P coated tetrapod-shaped ZnO nano- and microstructures

Mohd Najim,[ac] Gaurav Modi,[ab] Yogendra Kumar Mishra,[*b] Rainer Adelung,[b] Dharmendra Singh,[*cd] Vijaya Agarwala[a]

[a]*Department of Metallurgical and Materials Engineering, Indian Institute of Technology Roorkee, Roorkee, 247667, Uttarakhand, India*

[b]*Functional Nanomaterials, Institute for Materials Science, Christian-Albrechts University Kiel, Kaiserstr. 2, D-24143, Kiel, Germany*

[c]*Department of Electronics and Communication Engineering, Indian Institute of Technology Roorkee, Roorkee, 247667, Uttarakhand, India*

[d]*Centre of Excellence: Nanotechnology, Indian Institute of Technology Roorkee, Roorkee, 247667, Uttarakhand, India*

[*]Corresponding Authors: Dr. Yogendra Kumar Mishra (ykm@tf.uni-kiel.de)
Dr. Dharmendra Singh (dharmfec1@gmail.com)

Abstract

A viable lightweight absorber is the current need for stealth technology as well as microwave absorptions. Several microwave absorbers have been developed, but it is still a challenge to fabricate such an absorber that facilitates microwave absorption in broad bandwidth or covers the maximum portion of the frequency range 2-18 GHz, the commonly used range for radar and other applications. Therefore, it is highly required to develop a wide bandwidth absorber that can provide microwave absorption in the most part of the frequency range 2-18 GHz while simultaneously being lightweight and can be fabricated in desired bulk quantities by the cost-effective synthesis methods. In this paper, an attempt has been made to design an ultra-wide bandwidth absorber with enhanced microwave absorption response by using nickel-phosphorus coated tetrapod-shaped ZnO (Ni-P coated T-ZnO). In the Ni-P coated T-ZnO absorber, ZnO acts as a good dielectric contributor while Ni as a magnetic constituent to obtain a microwave absorbing composite material which is having favorable absorption properties. Ni-P coated ZnO nano-microstructures are synthesized by a simple and scalable two-step process; First, tetrapod-shaped ZnO (T-ZnO) structures have been grown by flame transport synthesis (FTS) approach in a single step process and then they have been coated with Ni-P by electroless coating technique. Their morphology, degree of crystallinity and existing phases were studied in detail by scanning electron microscopy (SEM), transmission electron microscopy (TEM), and X-ray diffraction (XRD) techniques. The complex permittivity and permeability of the "as-fabricated" T-ZnO and Ni-P coated T-ZnO have been measured in the frequency range of 4–14 GHz and their microwave absorption properties are computed with coaxial transmission-reflection method. The strongest reflection loss (RL) peak value of -36.41 dB has been obtained at a frequency of ~8.99 GHz with an absorber thickness of 3.4 mm for the Ni-P coated T-ZnO sample with a broad bandwidth of 10.0 GHz (RL < -10 dB) in the frequency range of 4.0-14.0 GHz.

Keywords: Microwave absorption, dielectric properties, ZnO tetrapods, flame transport synthesis, electroless Ni-P coating

1. Introduction

Microwave absorbing materials (MAM) have attracted worldwide attention because of their potentials to be used in a wide range of applications, such as in the aerospace and defense industries for stealth technology purposes.[1-2] The development of the first electromagnetic (EM) wave absorbing material could be traced back to 1930s, when a quarter wave resonant type absorber comprising of carbon black and TiO was created to improve the front-to-back ratio of the antenna.[3] Since then, there has been a considerable progress in the development of MAMs and a diverse range of materials has been tested, including dielectric absorbers e.g., carbonaceous materials,[4-9] conducting polymers,[10] ceramics,[11-13] and magnetic materials (ferrites),[14-16] graphene based hybrid materials,[17-18] and ultrafine metal powder.[19] Much of the research efforts in MAMs have been focused on designing an absorber with wide bandwidth, lightweight, lower thickness, and superior microwave absorption properties, but it is still very difficult to realize an absorber which exhibits all of the aforementioned characteristics simultaneously.

The absorption properties of a microwave absorber are contingent on its relative complex permeability (μ_r), permittivity (ε_r), electromagnetic impedance match, and the frequency of operation (f).[20] An ideal absorbing material must fulfill two fundamental requirements, first is that the incident EM wave should enter the absorber to a maximum extent (impedance match characteristic).[21] In order to achieve this, the intrinsic impedance (Z_{in}) of the material, which is estimated by relative permeability (μ_r), relative permittivity (ε_r), frequency (f), etc., and expressed by equation 1, should match with the impedance of free space, i.e., ~377 Ω.

$$Z_{in} = Z_0\left(\frac{\mu_r}{\varepsilon_r}\right)^{\frac{1}{2}} \tanh\left[j\left(\frac{2\pi fd}{c}\right)(\mu_r\varepsilon_r)^{\frac{1}{2}}\right] \qquad (1)$$

where Z_o is the impedance of free space, f is the frequency of EM wave, d is the thickness of absorber, and c is the velocity of light. Second prerequisite is that the incident EM wave should almost be completely attenuated within the absorber material (attenuation characteristic).[22] When the EM waves are incident on a dielectric material, formation and alignment of electric dipoles occur, resulting in absorption of EM energy.[23] The real part of permittivity takes care of the ability of the material to store the energy, however, the complex part is solely responsible for energy dissipation. Dielectric absorbers have got the advantage of being lightweight when

compared to their metallic counterparts.[24] Metallic magnetic materials are quite beneficial considering their large saturation magnetization and higher frequency Snoek's limit, which facilitates fabrication of thin absorbers with broad bandwidth,[25-28] however, magnetic material absorbers also exhibit certain limitations. Their permeability decreases sharply in the GHz frequency range owing to the increased eddy current losses on interaction with microwaves and its low resistivity.[29] A viable solution to this difficulty can be the fabrication of composite materials having dual components, one is the metallic magnetic component while other being some dielectric material.

A significant correlation does exist between the particle size and microwave absorption characteristics of any material.[30] Reduction in particle size not only augments the magnetic permeability of material, but also suppresses the eddy current phenomena, if the size is lesser than the skin depth (penetration depth) value for that material.[31] Thus, it is apparent that smaller particle size imparts some unique properties to the absorbing materials and hence nano-composites appear to be the ideal material candidates for the fabrication of microwave absorbers. There has been considerable research going on in the field of composite nanomaterials for microwave absorption. Liu et al.[32] utilized arc discharge method for the synthesis of ZnO coated Fe-nanocapsules and report a minimum RL value of ~-57.1 dB at 7.8 GHz and bandwidth in the frequency range of 6.1–15.7 GHz (RL<-10 dB) for an absorber thickness ranging from 1.5 mm to 5 mm. Recently, Wang et al.[33] studied the microwave absorption properties of ZnO coated with Ni nanoparticles by atomic layer deposition technique and reports a bandwidth of ~5.3 GHz (RL<-10 dB) and peak RL value of ~-48 dB at 10.4 GHz. However, the synthesis strategies followed by both of them exhibit issues like involvement of very complex and multistep fabrication procedures, and mass-scale productions, etc. The nano-composite fabrication method proposed herein is relatively very simple, a cost-effective process, and can be easily scaled up to obtain the desired quantities of the final product for real applications.[34]

It is evident that an ideal microwave absorbing material should be designed in a manner such that it has a high RL at minimal absorber thickness and operates in a wider frequency range. This amalgamation of properties can be achieved by synthesizing a nano-composite of magnetic and dielectric materials in a way that it exhibits a favorable combination of absorption

characteristics from both of the individual components. Nickel as a magnetic absorbent, has extensively been studied by many researchers, owing to its high permeability, large saturation magnetization, ease of preparation, and low cost, etc.[35-36] ZnO material has got wider applicability as a dielectric absorbent because of its light weight, semiconducting and piezoelectric features[37-39] as well as surface electric polarization effect[25] which is beneficial for microwave absorption. Tetrapod morphology of ZnO is particularly very unique as it exhibits nanoscale features in a three dimensional (3D) shape which can be directly utilized in several ways, for instance UV and stress sensors,[40-41] advance linkers,[42] biomedical engineering,[43-45] or in the form of multifunctional composites with unique properties.[46-47] These unique features of ZnO tetrapods motivated us to use them as microwave absorbing materials as they have been rarely used in this respect, in fact from literature search reveals only very few studies. Earlier investigations on the microwave absorption properties of tetrapod-shaped ZnO based absorbers by Jian et al.[48] and Zhang et al.[49] showed a remarkable improvement in the EM wave loss characteristics, which indeed demonstrate their huge potential for utilizations in this field. In present work, core-shell type Ni-P coated T-ZnO nano-microstructures have been fabricated and investigated in detail for their effectiveness in microwave absorption behaviour. Although a recent report exists on the microwave absorption of Ni coated ZnO synthesized by sophisticated atomic layer deposition approach,[33] it is difficult to find such type of work which has been done pertaining to synthesis of Ni-P coated on complex shaped ZnO structures, especially tetrapod-shaped ZnO, by a cost effective approach for their use in microwave absorption. Here, tetrapod shaped ZnO nano-microstructures were synthesized by a scalable and single step simple flame transport synthesis (FTS) approach[34] and were subsequently coated with nickel-phosphorus by using the electroless coating technique.[50] The fabricated nano-microstructures have been characterized in detail by using SEM for morphology and structural analysis, XRD for phase analysis, energy dispersive X-ray spectroscopy (EDS) for elemental analysis, TEM for morphological and crystallinity studies, and vector network analyzer (VNA) for measurement of the microwave absorption properties of the samples. The Ni-P coated T-ZnO demonstrated excellent microwave absorption characteristics as compared to "as-fabricated" T-ZnO, which can be primarily attributed to the enhanced interfacial polarization, better EM matching and magnetic loss contribution from the Ni-P coating on T-ZnO.

2. Experimental Details

As mentioned already that an ideal microwave absorbing material should consist of both the magnetic as well as the dielectric components. Here the ZnO tetrapods have been synthesized and coated with nickel-phosphorus to enhance its microwave absorption characteristics. Step wise fabrication procedure has been discussed in the following sub-sections:

2.1. Materials utilized

Commercial zinc powder (particle diameter ~3–5 μm, 99.0%) was purchased from GoodFellow, UK and polyvinyl butyral (PVB) was procured from Kuraray Europe GmbH, Germany. $SnCl_2$ (≥ 98.0 %), $Na_3C_6H_5O_7$ (≥ 98.0 %), $(NH_4)_2SO_4$ (≥ 99.5 %) and NH_4Cl (≥ 99.8 %) were obtained from HiMedia Laboratories Pvt. Ltd (India). $NiSO_4.6H_2O$ (≥ 98.0%) and $NaH_2PO_2.H_2O$ (≥ 99.0 %) were purchased from Loba Chemie. Reagent grade $PdCl_2$ was procured from Merck Ltd. and laboratory reagent grade ammonia solution (25.0 % as NH_3) from Rankem (India) was used. Deionized (DI) water was obtained from a Millipore water purifier system (Synergy Millipore, Merck). All solutions were prepared in DI water and all chemicals were used in as-received condition without any further purifications.

2.2 Synthesis of ZnO tetrapods

Tetrapod-shaped ZnO nano-microstructures were fabricated through the novel flame transport synthesis (FTS) technique developed by Mishra et al.[34] in a single growth step without the use of any catalysts. A ceramic crucible filled (~ 75 % volume) with Zn: PVB mixture (in 1:2 weight ratio) was inserted in a preheated furnace (simple muffle type) at 450 °C and then growth process was continued at 900 °C for 30 minutes. The sacrificial polymer PVB provides the control over local environmental conditions and growth of ZnO tetrapods occurs from transformed Zn vapor generated due to high temperature in the furnace. The growth mechanisms and applications of these nano- and microscale ZnO tetrapods by FTS process have been discussed in detail in previous papers.[51-52] ZnO tetrapods synthesized at 900 °C for 30 minutes have particularly been utilized here for fabricating the microwave absorbing materials.

2.3 Electroless deposition of Ni/P on T-ZnO

The electroless plating bath consisted of $NiSO_4.6H_2O$ (30 g/l) as source of nickel, $Na_3C_6H_5O_7$ (100 g/l) as complexing agent, $NaH_2PO_2.H_2O$ (20 g/l) as reducing agent, $(NH_4)_2SO_4$ (25 g/l) and NH_4Cl (25 g/l) as stabilizers, and ammonia solution to maintain the pH value of the electroless bath solution at 9.0.[53] Electroless deposition of Ni-P on ZnO tetrapods requires the creation of catalytic sites on the surface of T-ZnO which was achieved by pretreating the "as-fabricated" T-ZnO through sensitization and activation.[53] The sensitization of T-ZnO was carried out by immersing it in 0.1 % $SnCl_2$ solution for 3 min followed by subsequent activation in 0.01 % $PdCl_2$ solution for 5 min. It should be noted that after each pretreatment step, T-ZnO was washed thoroughly with DI water before proceeding to the subsequent step. The basic mechanism behind this two-step pretreatment method is that, first the Sn^{+2} ions are adsorbed on the surface of ZnO during the sensitization treatment which subsequently get displaced by the Pd^{+2} ions on activation. The Pd particles, eventually formed on the surface, serve as the catalytic sites for the electroless deposition of Ni-P on the ZnO surface.[54] The pretreated T-ZnO powder was immersed in 200 cm^3 of electroless Ni-P plating solution. The electroless deposition was carried out at a temperature of 80 ^oC for 40 minutes. The resulting ZnO nano-microtetrapods with a Ni-P coating were filtered, washed thoroughly with DI water, and dried at 60 ^oC. The reactions occurring on the catalytically active surface of T-ZnO leading to the electroless coating of Ni-P can be described by equations 2 and 3.[55] The process of synthesis of Ni-P coated T-ZnO, by electroless coating technique, has been schematically illustrated in Fig. 1.

$$Ni^{+2} + H_2PO_2^- + H_2O \rightarrow Ni + 2H^+ + H\left(HPO_3\right)^- \qquad (2)$$

$$HPO_2^- + H_2O \rightarrow H\left(HPO_3\right)^- + \frac{1}{2}H_2 \qquad (3)$$

2.4 Characterization of "as-fabricated" T-ZnO and Ni-P coated T-ZnO

The SEM (Zeiss) was used to examine the morphology of the "as-fabricated" T-ZnO, pretreated T-ZnO (after sensitization and activation) and Ni-P coated T-ZnO. XRD was performed to identify the phases present in "as-fabricated" T-ZnO and Ni-P coated T-ZnO using a Rigaku X-Ray diffractometer with Cu Kα radiation (λ = 0.154 nm) at 40 KV and 40 mA. The angular 2θ range was set from 20-110^o while the scan rate was kept at 2 degrees/min. Scherrer formula was applied to calculate the average crystal lattice parameters from the diffraction peaks. Elemental composition of the Ni-P coated T-ZnO nano-microstructures was determined using

EDS. Selected area electron diffraction (SAED) pattern of the "as-fabricated" T-ZnO and Ni-P coated T-ZnO was obtained using TEM (20 Tecnai G^2).

The electromagnetic parameters and microwave absorption properties of "as-fabricated" T-ZnO and Ni-P coated T-ZnO nano-microstructures were computed with coaxial transmission-reflection method. The samples were mixed with an epoxy resin (Bisphenol A Novolac) binder (powder to epoxy ratio 90:10) and casted in the shape of a hollow cylinder by dye casting method. The experimentally measured dielectric constant of cured epoxy was in the range of 1.76–1.68 for 4.0-14.0 GHz. The cylindrical-shaped pellets were having the dimensions of 3.05 mm inner diameter and 7.00 mm outer diameter with 5 mm height for 50 Ω Airline (Agilent 85055A type-N verification kit). Based on the scattering parameters of the cylindrical-shaped samples, the complex permeability and permittivity were measured by a VNA (Agilent N5224A) in the frequency range of 4–14 GHz at room temperature using Nicolson models.[56] The RL curves of T-ZnO and Ni-P coated T-ZnO at a particular frequency and given absorber thickness were derived using relative complex permeability and permittivity through equations 1 and 4. The term Z_{in} in equation 4 represents the impedance of the absorber while Z_o is the impedance of the free space.

$$RL = 20 \log \left[\frac{|Z_{in} - Z_0|}{|Z_{in} + Z_0|} \right] \qquad (4)$$

3. Results and discussion

3.1 Morphology and elemental analysis of "as-fabricated" and Ni-P coated ZnO tetrapods

The "as-fabricated" T-ZnO from flame transport synthesis is in the form of a white fluffy powder (supporting information Fig. S1a). The SEM morphologies of the "as-fabricated" T-ZnO and Ni-P coated ZnO nano-microtetrapods are shown in Fig. 2. The tetrapods are observed to have nearly uniform hexagonal cylindrical arms and are terminated in smaller hexagonal tips (indicated by circular region in Fig. 2b). The tetrapod-shaped ZnO structure typically has an arm diameter of about 4 μm at its base and the tip diameter is observed to vary from few hundred nanometers to 1 μm. The typical length of the arms associated with the tetrapods is in the range of 15-20 μm. The well faceted hexagonal morphology of the tetrapod arms is clearly evident from the SEM images which is again an indication of high crystalline nature of these structures with c-axis as a preferred growth direction of the hexagonal unit cell.

The "as-fabricated" ZnO tetrapods were subjected to Ni-P coating by electroless deposition technique. The color of the powder changed from white to yellowish-brown after the pretreatment step and to grayish-black after electroless deposition of Ni-P (supporting information Fig. S1 b-c). Fig. 2(c-d) show the representative SEM image of T-ZnO after the pretreatment steps of sensitization with $SnCl_2$ and activation with $PdCl_2$ solutions. A clear distinction in the surface morphology for the pretreated T-ZnO can be observed when compared with the "as-fabricated" T-ZnO. The pretreated T-ZnO appears to have some nucleation sites attached to its surface. This observation confirms the validity of the used pretreatment procedure prior to the electroless coating with Ni-P layers. The typical SEM images of the Ni-P coated T-ZnO is shown in Fig. 2(e-f) which reveal that the arms of T-ZnO (visible as rod-like structures and indicated by arrow in Fig. 2(e) are coated uniformly with Ni-P material (after electroless deposition). A further magnified SEM image from Fig. 2(e), corresponding to a typical Ni-P coated T-ZnO arm, is shown in Fig. 2(f), and it clearly illustrates the formation of globules of coating on the T-ZnO surface. The Ni-P coated T-ZnO arms can be easily distinguished from the "as-fabricated" T-ZnO and pretreated T-ZnO. Reproducibility of the electroless Ni-P coating on T-ZnO was confirmed further experiments followed by SEM studies.

The elemental composition of the Ni-P coated T-ZnO nano-microstructures has been evaluated using EDS corresponding to the region (marked square) indicated in Fig. 2(f) and the results are shown in Fig. 3. The indicated region is observed to have a high percentage of electrolessly deposited nickel while the presence of Zn is about 8.38 % (atomic %). The almost zinc is present in the form of ZnO, therefore mainly ZnO and Ni peaks are observed in the XRD pattern of Ni-P coated T-ZnO (Fig. 4) specimen. Since the stoichiometric ratio of zinc to oxygen in ZnO is 1:1, it can be evaluated that the ZnO present in the sample is about 16.76 % (atomic %). The remaining oxygen is most likely to be associated with some nickel (slightly oxidized due to increased reactivity in nanoscale range) or phosphorus (in the form of P_2O_5).

3.2 XRD and TEM investigations

The phases present in "as-fabricated" T-ZnO and Ni-P coated T-ZnO were investigated by means of XRD. Fig. 4 displays the typical XRD pattern obtained from the as-synthesized T-ZnO which reveals that the main XRD peaks are (100), (002), and (101) of hexagonal wurtzite

crystal structure of ZnO. The XRD peaks are an indication of the high degree of crystallinity of the synthesized ZnO tetrapods.[57] The value of the lattice parameter calculated for tetrapod-shaped ZnO using the Scherrer formula is 2.601 Å, which is almost equal to the lattice parameter value of 2.602 Å for bulk ZnO without any strain. It implies that a negligible amount of strain exists in the nano-microstructures and reinforces the fact that the tetrapods have a high degree of crystallinity. The XRD pattern obtained from the Ni-P coated T-ZnO is also illustrated in Fig. 4, which indicates that in addition to the peaks corresponding to ZnO, there is a new broad peak at around $2\theta = 45^{o}$, which originates from the electrolessly deposited Ni-P layers. The results of the XRD analysis clearly indicate the successful deposition of Ni–P layers onto the surfaces of T-ZnO by the electroless coating process and also confirm the amorphous state of the Ni–P coating. The obtained results are in good agreement with those already reported in literature.[58]

Fig. 5 illustrates the TEM studies carried out on the "as-fabricated" T-ZnO (Fig. 5a-c) and Ni-P coated T-ZnO (Fig. 5d-f). Fig. 5(a) displays a typical T-ZnO arm which reveals that the arm diameter abruptly decreases near the tips with diameter in the range of 250-300 nm as was also observed in SEM (Fig. 2a-b). Fig. 5(b) depicts an arm of T-ZnO with a broken tip and the SAED pattern obtained from the T-ZnO tip is shown in Fig. 5(c). On indexing, the SAED pattern is confirmed to be of single crystalline ZnO with beam direction [10-1].[59] The morphology and phase structure of the Ni-P coated T-ZnO has also been revealed by TEM investigations. Fig. 5(d-e) show the representative TEM images of the broken tips of the T-ZnO arms with Ni–P coating and Fig. 5(f) depicts the electron diffraction pattern selectively taken on the edge of Ni-P coated T-ZnO (circular point). The TEM images clearly indicate that the Ni–P layer (visible as lighter layer surrounding the darker region) almost uniformly covers the arm of T-ZnO. The amorphous nature of the electroless Ni-P coating is confirmed from the diffused ring SAED pattern shown in Fig. 5(f) and it further supports the results obtained from XRD (Fig. 4). The diffused ring SAED pattern reveals the presence of Ni crystallites embedded in an amorphous Ni matrix. From TEM observations, it is confirmed that T-ZnO has been successfully coated with amorphous Ni–P layers.

3.3 Microwave absorption characteristics of "as-fabricated" T-ZnO and Ni-P coated T-ZnO

The complex permeability and permittivity of "as-fabricated" T-ZnO and Ni-P coated T-ZnO nano-microstructures are determined using a transmission line method with VNA in the 4-14 GHz frequency range and corresponding results are shown in Fig. 6. Complex permittivity and permeability are the fundamental parameters required for the evaluation of microwave absorption properties of an absorber.[22] The maximum values of real (ε') and imaginary (ε'') parts of permittivity for Ni-P coated T-ZnO are observed as 4.25 at 4.0 GHz and 2.52 at 14.0 GHz, respectively, and are higher than for "as-fabricated" T-ZnO (ε' 3.98 at 4.0 GHz and ε'' 0.82 at 14.0 GHz). It is found that the real part of permeability (μ') for "as-fabricated" T-ZnO is having a constant value of 0.98 for the frequency range of 4.0 to 14.0 GHz and the highest value is noticed for Ni-P coated T-ZnO 0.80 at 4.0 GHz. The maximum values of imaginary part of permeability (μ'') for "as-fabricated" T-ZnO and Ni-P coated T-ZnO are found to be 0.04 at 14.0 GHz and 1.56 at 6.5 GHz respectively. The imaginary permittivity (ε'') is observed to have almost the same value for both the samples up to a frequency of 10 GHz, but afterwards it increases steeply reaching a value of ~2.52 at 14 GHz, henceforth enhancing the dielectric losses for Ni-P coated T-ZnO. Likewise, the imaginary permeability (μ'') of Ni-P coated T-ZnO displays a significantly higher value in the 4-14 GHz frequency range in comparison to "as-fabricated" T-ZnO sample, which indicates a higher magnetic loss for Ni-P coated T-ZnO. Additionally, μ'' exhibits a resonance peak at 6.5 GHz for Ni-P coated T-ZnO, which can be associated with the natural resonance of nickel and it further contributes to the enhancement of its microwave absorption performance.[35, 60] The increased value of imaginary parts (ε'' and μ'') for Ni-P coated T-ZnO leads to good losses, as shown in Fig. 6(a-d) and Fig. 7(a-b).

The loss tangents of the synthesized samples have been plotted and are shown in Fig. 7. It can be observed that the dielectric loss tangents are almost similar for both the samples in the frequency range of 4-10 GHz, but with increase in frequency from 10-14 GHz, the dielectric loss tangent is found to increase exponentially for Ni-P coated T-ZnO. On the other hand, the magnetic loss tangent seems to exhibit a much higher value for Ni-P coated T-ZnO in the 4-14 GHz frequency range, reaching a peak value of ~ 2 at ~6.5 GHz, after which they appear to approach a common value. From the aforementioned observations, it can be visualized that magnetic losses are dominating at lower frequencies while the dielectric losses dominate at

higher frequencies in NiP coated T-ZnO specimen.[61] It also confirms the efficient complementaries existing between the magnetic and dielectric losses for the Ni-P coated T-ZnO. The total loss in an absorber is the aggregate of the magnetic and dielectric losses. The synergistic effect between the dielectric and magnetic losses eventually results in the excellent microwave absorption properties of the Ni-P coated T-ZnO absorber. Various types of magnetic losses like natural resonance, domain-wall displacement etc. may be present in Ni-P coated T-ZnO sample.[26, 32]

The enhanced losses for the Ni-P coated T-ZnO can be ascribed to its core-shell structure. ZnO is a dielectric material, where the loss mechanism is believed to be resulting from the dipolar polarization and the relaxation phenomena associated with it.[62] However, when such a dielectric material is coated with some other materials, new interfaces are created which introduce additional polarization charges at the surface and the dielectric relaxation behaviour of the absorber becomes highly complex.[63] Moreover, in present investigations it has been found that the Ni-P coating is amorphous in nature and has nanocrystallites of Ni embedded in an amorphous Ni matrix (Fig. 5d-f), which contributes additional interfaces, too. It has been reported in literature that the property of interfaces play a significant role in determining the dielectric performance.[64] The real part of complex permittivity is a measure of the polarization capability while the imaginary part determines the dielectric loss of a material.[65] The mechanisms responsible for dielectric loss can be categorized as electron polarization, ionic polarization, interfacial polarization, and electric dipolar polarization.[66] Here, due to the existence of metallic Ni shells, electrons can travel freely within it and accumulate at the ZnO/Ni-P coating interface, forming a structure similar to a boundary-layer capacitor[67] and resulting in interfacial electric dipolar polarization. Interfacial polarization also occurs within the Ni-P coating at interfaces between the crystallites of Ni embedded in an amorphous Ni matrix. Thus in this case, the interfacial polarization[68] and the associated relaxation phenomena constitute a very important loss mechanism. It is speculated that the total dielectric loss has significant contributions from the polarization and interfacial polarization phenomena. Further, the small sized T-ZnO particles have a relatively large effective surface area which accounts for an increase in the electric polarization at the particle surface and enhances the scattering intensity for microwave.

The RL has been calculated for "as-fabricated" T-ZnO and Ni-P coated T-ZnO by using equations 1 and 4. The thickness (*d*) has been varied from 0.5-5.0 mm at the interval of 0.1 mm for RL calculations. Fig. 8 illustrates the variation in RL with frequency and absorber thickness for "as-fabricated" T-ZnO and Ni-P coated T-ZnO. The ideal combination of RL value, bandwidth, and absorber thickness can be conveniently estimated from Fig. 8.

Fig. 9 shows the RL curves for both the samples at their optimum absorber thickness of 2.6 mm and 3.4 mm, respectively. It can clearly be observed from the RL curves that very less microwave absorption, i.e., -7.87 dB occurs in the case of pure T-ZnO, while for the Ni-P coated T-ZnO, a peak RL value of -36.41 dB has been achieved with a broad bandwidth of 10.0 GHz (<-10 dB) from 4.0-14.0 GHz frequency range at 3.40 mm absorber thickness.

The observed outstanding microwave absorption properties of the Ni-P coated T-ZnO can be attributed to the various possible mechanisms. An ideal microwave absorber is characterized by efficient complementaries between the relative permittivity and permeability in the absorbing materials.[23] For this condition of EM matching to be fulfilled, both magnetic and dielectric loss should take place in the absorber. The heterogeneous system of Ni-coated T-ZnO facilitates a better EM matching because of the presence of Ni shells on the T-ZnO. The excellent microwave absorption properties can be attributed to the appropriate EM matching[69] and the multipolarization of the interfaces between Ni-P coating/T-ZnO and crystallites of Ni embedded in an amorphous Ni matrix. The overall loss in the EM wave occurs via a number of possible mechanisms operating together in a coherent manner. For example, tetrapod-shaped ZnO structure exhibits arms with diameter belonging to the nanoscale range because of which quantum confinement effects could also considerably contribute to change in microwave absorption properties. As per Kubo theory[69], quantum confinement effect causes the energy levels in T-ZnO to split and become discrete instead of being continuous. So, when the microwaves are incident over T-ZnO based absorbers, the electron absorbs a photon and moves to a higher energy level. Moreover, the defects and suspending band lead to multiple scattering and interface polarization resulting in the absorption of the EM wave. Additionally, a unique feature of T-ZnO is that it possesses isotropic crystal symmetry, as a result of which it can form

isotropic quasiantennas and cellular networks in T-ZnO based absorbers.[70-71] The EM wave penetrates the discontinuous network and energy is induced into a dissipative current which gradually diminishes in the discontinuous cellular networks resulting in energy attenuation.[37, 72] Moreover, the piezoelectric nature of ZnO may also be contributing to the attenuation of energy of the EM wave.

4. Conclusions

In this paper, tetrapod-shaped ZnO nano-microstructures were synthesized by using the novel flame transport synthesis approach and were successfully coated with Ni-P using the electroless coating process to form a unique core-shell structure. The uniformity of the Ni-P coating and its amorphous nature were confirmed by SEM, TEM, and XRD investigations. The electromagnetic properties are investigated which reveal that the losses are enhanced for the Ni-P coated T-ZnO based absorber as compared to pure T-ZnO it could be due to a better EM matching between T-ZnO and Ni-P coating. The microwave absorption value and bandwidth are enhanced greatly for the Ni-P coated T-ZnO. The absorption value increased from -7.87 dB (d = 2.6 mm) to -36.41 dB (d = 3.4 mm) while an ultra-wide bandwidth of 10.0 GHz (4.0-14.0 GHz for RL < -10 dB) has been successfully achieved. The excellent absorption properties of the Ni-P coated T-ZnO are speculated to be a collective outcome of the interfacial electric dipolar polarization, efficient complementaries between relative permittivity and permeability, various magnetic losses, and the distinctive properties of the small-sized T-ZnO core. The Ni-P coated T-ZnO based ultra-wide bandwidth absorber exhibits a great potential to be utilized for stealth technology applications and electromagnetic interference (EMI) reduction.

Acknowledgements

MN is thankful to Ministry of Human Resources and Development (MHRD), India, for giving fellowship grant. GM acknowledges DAAD, Germany, for fellowship under DAAD-WISE program to visit and work at University of Kiel. YKM and RA acknowledge the financial support from German Research Foundation (DFG) under scheme PAK 902 (AD 183/16-1). DS and VA acknowledge Defense Research and Development Organization (DRDO), Delhi, India, for funding.

5. References

1. P. Y. Chen, J. Soric and A. Alu, *Adv. Mater.*, 2012, **24**, OP281-OP304.
2. T. Xia, C. Zhang, N. A. Oyler and X. Chen, *Adv. Mater.*, 2013, **25**, 6905-6910.
3. N. V. Machinerieen, *French Patent*, 1936, **802**, 728.
4. R. Che, L. M. Peng, X. F. Duan, Q. Chen and X. Liang, *Adv. Mater.*, 2004, **16**, 401-405.
5. Z. Liu, G. Bai, Y. Huang, F. Li, Y. Ma, T. Guo, X. He, X. Lin, H. Gao and Y. Chen, *J. Phys. Chem. C*, 2007, **111**, 13696-13700.
6. Q. Liu, D. Zhang and T. Fan, *Appl. Phys. Lett.*, 2008, **93**, 013110.
7. Q. Liu, J. Gu, W. Zhang, Y. Miyamoto, Z. Chen and D. Zhang, *J. Mater. Chem.*, 2012, **22**, 21183-21188.
8. M. Najim, P. Smitha, V. Agarwala and D. Singh, *J. Mater. Sci.: Mater. Electron.*, 2015, (DOI: 10.1007/s10854-10015-13366-10858).
9. R. Panwar, P. Smitha, V. Agarwala and D. Singh, *IEEE Trans. Magn.*, 2015, **(In Press)**.
10. A. Ohlan, K. Singh, A. Chandra and S. K. Dhawan, *ACS Appl. Mater. Interfaces*, 2010, **2**, 927-933.
11. F. Xia, J. Liu, D. Gu, P. Zhao, J. Zhang and R. Che, *Nanoscale*, 2011, **3**, 3860-3867.
12. M. Najim, P. Smitha, V. Agarwala and D. Singh, *Adv. Sci. Lett.*, 2014, **20**, 1490-1494.
13. R. Panwar, S. Puthucheri, V. Agarwala and D. Singh, *IEEE Trans. Microw. Theory Techn.*, 2015, (DOI: 10.1109/TMTT.2015.2446989)
14. J. Liu, R. Che, H. Chen, F. Zhang, F. Xia, Q. Wu and M. Wang, *Small*, 2012, **8**, 1214-1221.
15. Q. Liu, B. Cao, C. Feng, W. Zhang, S. Zhu and D. Zhang, *Compos. Sci. Technol.*, 2012, **72**, 1632-1636.
16. M. Fu, Q. Jiao and Y. Zhao, *J. Mater. Chem. A*, 2013, **1**, 5577-5586.
17. C. Hu, Z. Mou, G. Lu, N. Chen, Z. Dong, M. Hu and L. Qu, *Phys. Chem. Chem. Phys.*, 2013, **15**, 13038-13043.
18. L. Wang, Y. Huang, C. Li, J. Chen and X. Sun, *Phys. Chem. Chem. Phys.*, 2015, **17**, 5878-5886.
19. T. Wang, H. Wang, X. Chi, R. Li and J. Wang, *Carbon*, 2014, **74**, 312-318.
20. C. M. Watts, X. Liu and W. J. Padilla, *Adv. Mater.*, 2012, **24**, OP98-OP120.
21. N. Mattiucci, M. Bloemer, N. Aközbek and G. D'Aguanno, *Sci. Rep.*, 2013, **3**.
22. S. Wen, Y. Liu, X. Zhao, J. Cheng and H. Li, *Phys. Chem. Chem. Phys.*, 2014, **16**, 18333-18340.
23. A. Hoz and A. Loupy, *Microwaves in Organic Synthesis*, Wiley-VCH, Weinheim, 3rd edn., 2012.
24. X. Wang, X. Liao, W. Zhang and B. Shi, *Phys. Chem. Chem. Phys.*, 2015, **17**, 2113-2120.
25. J. Snoek, *Physica*, 1948, **14**, 207-217.
26. J. Snoek, *Nature*, 1947, **160**, 90.
27. L. Yan, J. Wang, Y. Ye, Z. Hao, Q. Liu and F. Li, *J. Alloys Compd.*, 2009, **487**, 708-711.
28. X. Gu, W. Zhu, C. Jia, R. Zhao, W. Schmidt and Y. Wang, *Chem. Commun.*, 2011, **47**, 5337-5339.
29. H. Hekmatara, M. Seifi, K. Forooraghi and S. Mirzaee, *Phys. Chem. Chem. Phys.*, 2014, **16**, 24069-24075.
30. L. Wu, J. Ding, H. Jiang, L. Chen and C. Ong, *J. Magn. Magn. Mater.*, 2005, **285**, 233-239.
31. X. Zhang, X. Dong, H. Huang, Y. Liu, W. Wang, X. Zhu, B. Lv, J. Lei and C. Lee, *Appl. Phys. Lett.*, 2006, **89**, 3115.
32. X. G. Liu, D. Y. Geng, H. Meng, P. J. Shang and Z. D. Zhang, *Appl. Phys. Lett.*, 2008, **92**, 173117.
33. G. Wang, X. Peng, L. Yu, G. Wan, S. Lin and Y. Qin, *J. Mater. Chem. A*, 2015, **3**, 2734-2740.
34. Y. K. Mishra, S. Kaps, A. Schuchardt, I. Paulowicz, X. Jin, D. Gedamu, S. Freitag, M. Claus, S. Wille, A. Kovalev, S. N. Gorb and R. Adelung, *Part. Part. Syst. Charact.*, 2013, **30**, 775-783.
35. B. Zhao, G. Shao, B. Fan, W. Zhao and R. Zhang, *Phys. Chem. Chem. Phys.*, 2015, **17**, 2531-2539.
36. B. Zhao, G. Shao, B. Fan, W. Zhao, Y. Xie and R. Zhang, *Phys. Chem. Chem. Phys.*, 2015, **17**, 8802-8810.
37. R. Zhuo, H. Feng, J. Chen, D. Yan, J. Feng, H. Li, B. Geng, S. Cheng, X. Xu and P. Yan, *J. Phys. Chem. C*, 2008, **112**, 11767-11775.

38. X.-Y. Fang, M.-S. Cao, X.-L. Shi, Z.-L. Hou, W.-L. Song and J. Yuan, *J. Appl. Phys.*, 2010, **107**, 054304.
39. L. Kong, X. Yin, F. Ye, Q. Li, L. Zhang and L. Cheng, *J. Phys. Chem. C*, 2013, **117**, 2135-2146.
40. X. Jin, M. Götz, S. Wille, Y. K. Mishra, R. Adelung and C. Zollfrank, *Adv. Mater.*, 2013, **25**, 1342-1347.
41. D. Gedamu, I. Paulowicz, S. Kaps, O. Lupan, S. Wille, G. Haidarschin, Y. K. Mishra and R. Adelung, *Adv. Mater.*, 2014, **26**, 1541-1550.
42. X. Jin, J. Strueben, L. Heepe, A. Kovalev, Y. K. Mishra, R. Adelung, S. N. Gorb and A. Staubitz, *Adv. Mater.*, 2012, **24**, 5676-5680.
43. H. Papavlassopoulos, Y. K. Mishra, S. Kaps, I. Paulowicz, R. Abdelaziz, M. Elbahri, E. Maser, R. Adelung and C. Röhl, *PLoS ONE*, 2014, **9**, e84983.
44. Y. K. Mishra, R. Adelung, C. Röhl, D. Shukla, F. Spors and V. Tiwari, *Antiviral Res.*, 2011, **92**, 305-312.
45. T. Antoine, Y. K. Mishra, J. Trigilio, V. Tiwari, R. Adelung and D. Shukla, *Antiviral Res.*, 2012, **96**, 363-375.
46. X. Jin, M. Deng, S. Kaps, X. Zhu, I. Hölken, K. Mess, R. Adelung and Y. K. Mishra, *PLoS ONE*, 2014, **9**, e106991.
47. G. Modi, *Adv. Nat. Sci.: Nanosci. Nanotechnol.*, 2015, **6**, 033002.
48. X. Jian, X. Chen, Z. Zhou, G. Li, M. Jiang, X. Xu, J. Lu, Q. Li, Y. Wang and J. Gou, *Phys. Chem. Chem. Phys.*, 2015, **17**, 3024-3031.
49. L. Zhang, X. Zhang, G. Zhang, Z. Zhang, S. Liu, P. Li, Q. Liao, Y. Zhao and Y. Zhang, *RSC Adv.*, 2015, **5**, 10197-10203.
50. R. C. Agarwala, *Pramana J. Phys.*, 2005, **65**, 959-965.
51. Y. K. Mishra, S. Kaps, A. Schuchardt, I. Paulowicz, X. Jin, D. Gedamu, S. Wille, O. Lupan and R. Adelung, *KONA Powder Part. J.*, 2014, **31**, 92-110.
52. Y. K. Mishra, G. Modi, V. Cretu, V. Postica, O. Lupan, T. Reimer, I. Paulowicz, V. Hrkac, W. Benecke and L. Kienle, *ACS Appl. Mater. Interfaces*, 2015, **7**.
53. R. Agarwala and V. Agarwala, *Sadhana*, 2003, **28**, 475-493.
54. S. Sharma, R. Agarwala, V. Agarwala and K. Satyanarayana, *J. Mater. Sci.*, 2002, **37**, 5247-5254.
55. K. H. Krishnan, S. John, K. Srinivasan, J. Praveen, M. Ganesan and P. Kavimani, *Metall. Mater. Trans. A*, 2006, **37**, 1917-1926.
56. A. Nicolson and G. Ross, *IEEE Trans. Instrum. Meas.*, 1970, **19**, 377-382.
57. B. D. Cullity and S. R. Stock, *Elements of X-ray Diffraction*, Prentice hall Upper Saddle River, NJ, 2001.
58. J. Balaraju, T. S. Narayanan and S. Seshadri, *Mater. Res. Bull.*, 2006, **41**, 847-860.
59. W.-T. Chiou, W.-Y. Wu and J.-M. Ting, *Diam. Relat. Mater.*, 2003, **12**, 1841-1844.
60. T. Chen, F. Deng, J. Zhu, C. Chen, G. Sun, S. Ma and X. Yang, *J. Mater. Chem.*, 2012, **22**, 15190-15197.
61. R. Sharma, R. Agarwala and V. Agarwala, *Mater. Lett.*, 2008, **62**, 2233-2236.
62. X. Dong, X. Zhang, H. Huang and F. Zuo, *Appl. Phys. Lett.*, 2008, **92**, 013127.
63. G. Wang, Y. Chang, L. Wang and C. Liu, *Adv. Powder Technol.*, 2012, **23**, 861-865.
64. T. Lewis, *J. Phys. D: Appl. Phys.*, 2005, **38**, 202.
65. P. Watts, D. Ponnampalam, W. Hsu, A. Barnes and B. Chambers, *Chem. Phys. Lett.*, 2003, **378**, 609-614.
66. B. Gao, L. Qiao, J. Wang, Q. Liu, F. Li, J. Feng and D. Xue, *J. Phys. D: Appl. Phys.*, 2008, **41**, 235005.
67. X. Zhang, P. Guan and X. Dong, *Appl. Phys. Lett.*, 2010, **96**, 223111.
68. C. Zhou, Q. Fang, F. Yan, W. Wang, K. Wu, Y. Liu, Q. Lv, H. Zhang, Q. Zhang and J. Li, *J. Magn. Magn. Mater.*, 2012, **324**, 1720-1725.
69. R. Kubo, *J. Phys. Soc. Japan*, 1962, **17**, 975-986.
70. H. Li, J. Wang, Y. Huang, X. Yan, J. Qi, J. Liu and Y. Zhang, *Mater. Sci. Eng. B*, 2010, **175**, 81-85.
71. Z. Zhou, L. Chu and S. Hu, *Mater. Sci. Eng. B*, 2006, **126**, 93-96.
72. H. Li, Y. Huang, G. Sun, X. Yan, Y. Yang, J. Wang and Y. Zhang, *J. Phys. Chem. C*, 2010, **114**, 10088-10091.

Figures & Captions

Figure 1

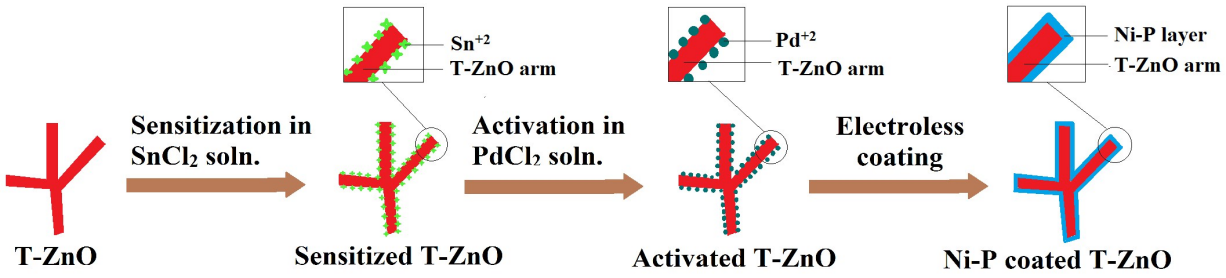

Figure 1. Schematic representation of the process of coating of T-ZnO nano- and micro tetrapod structures with Ni-P by the electroless deposition process.

Figure 2

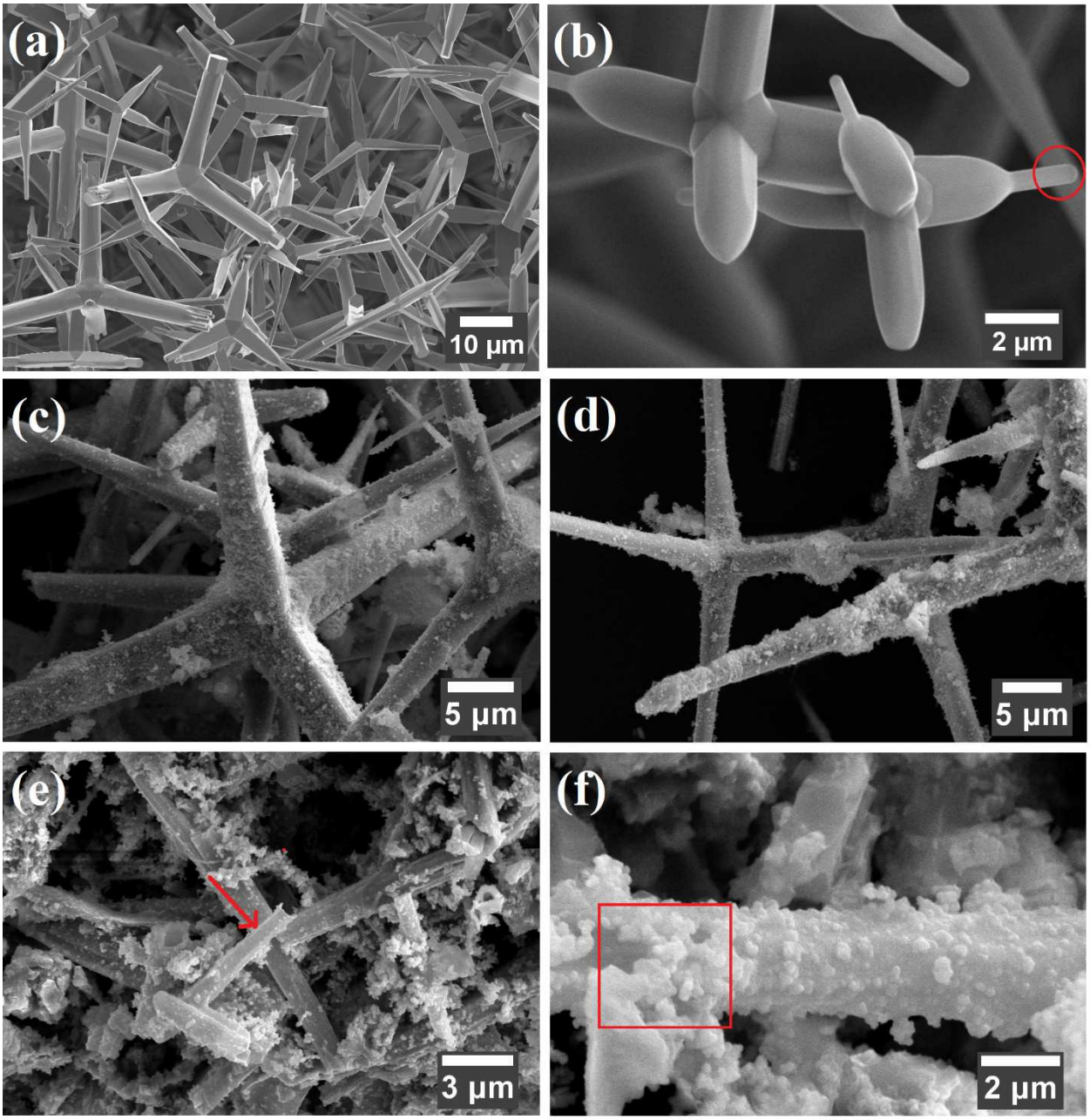

Figure 2. SEM images of (a) dense network of uniform "as-fabricated" T-ZnO, (b) magnified view of the "as-fabricated" T-ZnO network, (c-d) different regions of T-ZnO after sensitization and activation pretreatment, (e) Ni-P coated T-ZnO arms visible as rod-like structures (indicated by arrow), and (f) magnified image of a Ni-P coated T-ZnO arm (EDS spectra was taken from the indicated region).

Figure 3

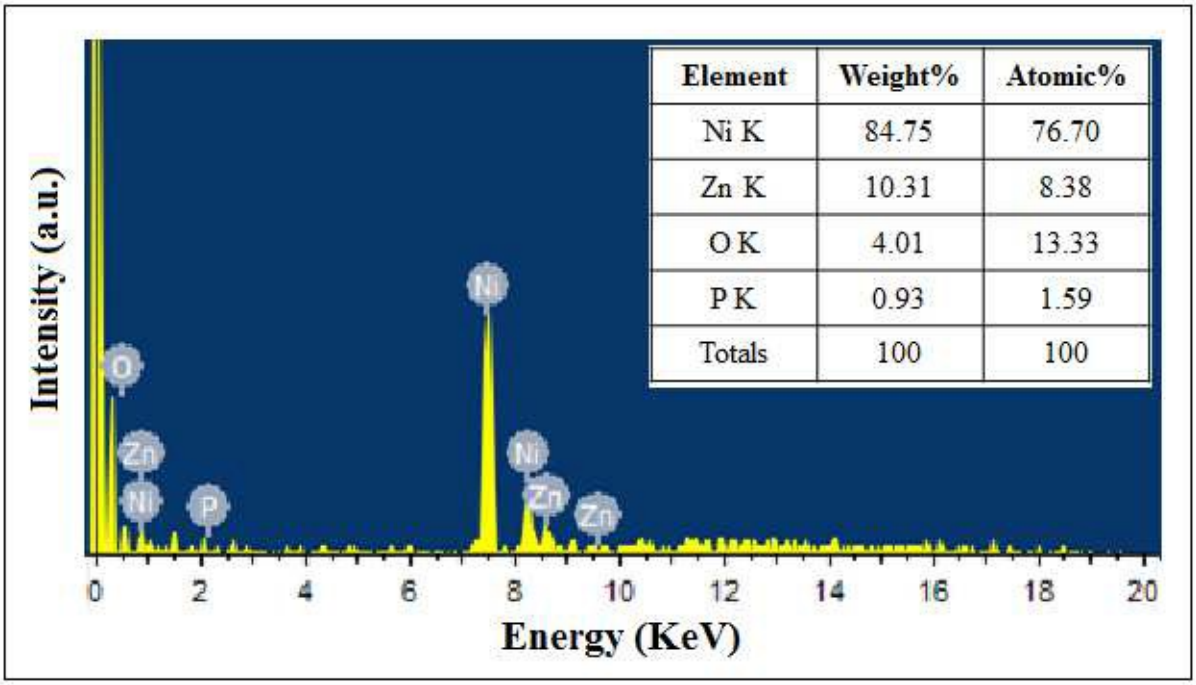

Element	Weight%	Atomic%
Ni K	84.75	76.70
Zn K	10.31	8.38
O K	4.01	13.33
P K	0.93	1.59
Totals	100	100

Figure 3. EDS spectrum of Ni-P coated T-ZnO showing the presence of Ni, P, Zn and O. Elemental composition of indicated region in Fig. 2(f) is shown in inset table.

Figure 4

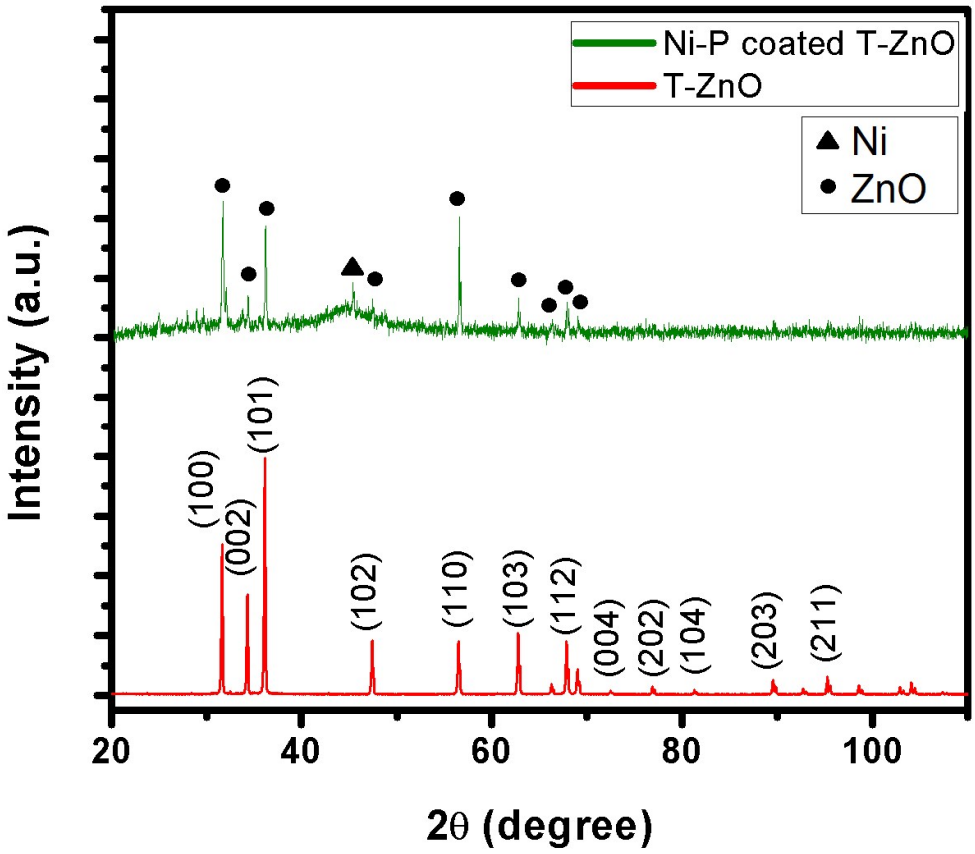

Figure 4. XRD spectrum of "as-fabricated" T-ZnO and Ni-P coated T-ZnO. An additional broad peak at $2\theta \approx 45^{o}$ corresponding to electrolessly deposited amorphous nickel is observed for Ni-P coated T-ZnO.

Figure 5

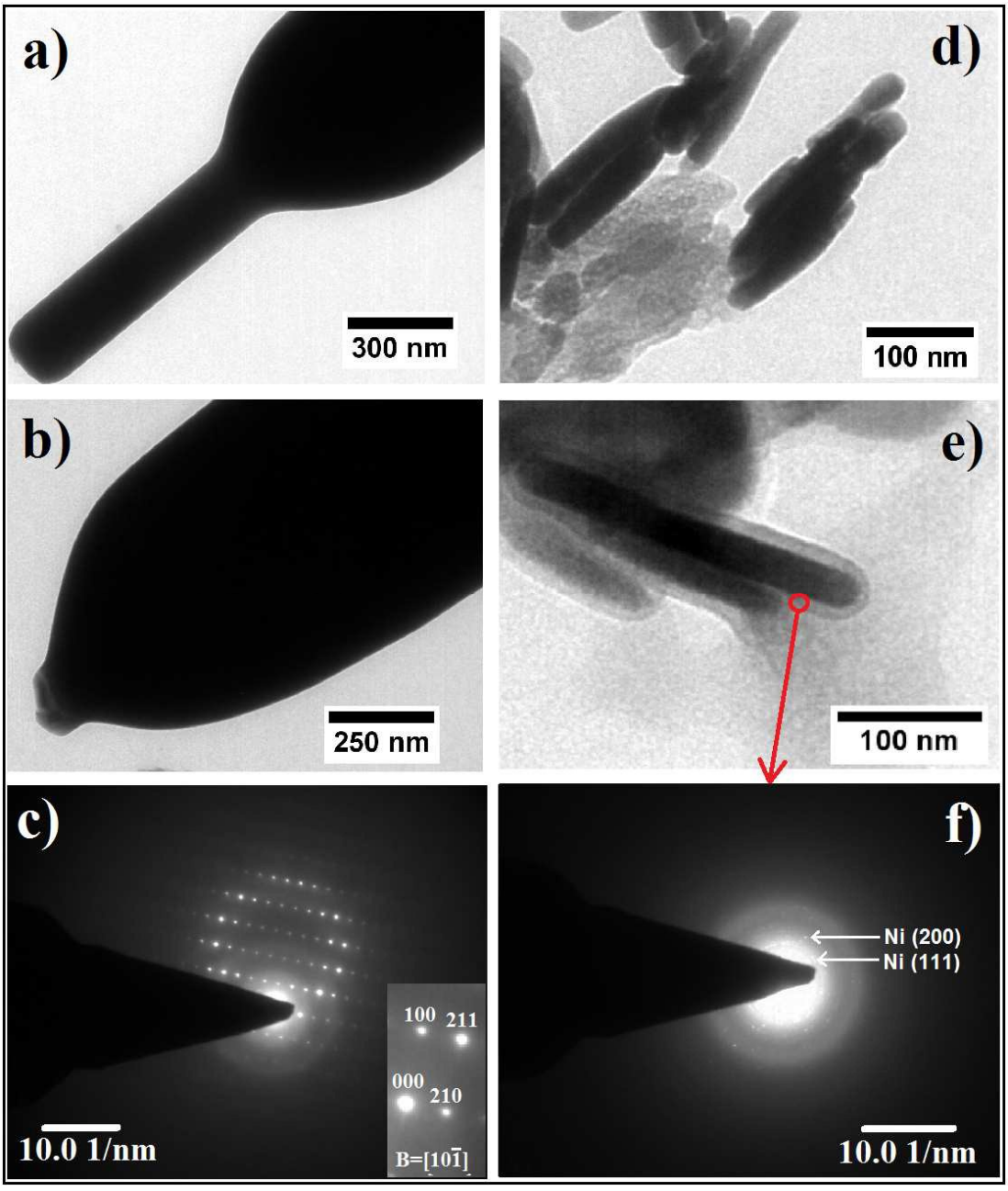

Figure 5. TEM images of (a-c) "as-fabricated" T-ZnO and (d-f) Ni-P coated T-ZnO. (a) bright field TEM image of a tetrapod arm with its tip intact, (b) bright field TEM image of a tetrapod arm with broken tip, (c) SAED pattern obtained from the tip of the "as-fabricated" T-ZnO, (d) bright field TEM image of clusters of broken tips of tetrapod arms with a layer of Ni-P coating on them, (e) bright field TEM image of a Ni-P coated broken T-ZnO arm tip, and (f) SAED pattern obtained from the Ni-P coating taken selectively from the region indicated in Fig. 5(e).

Figure 6

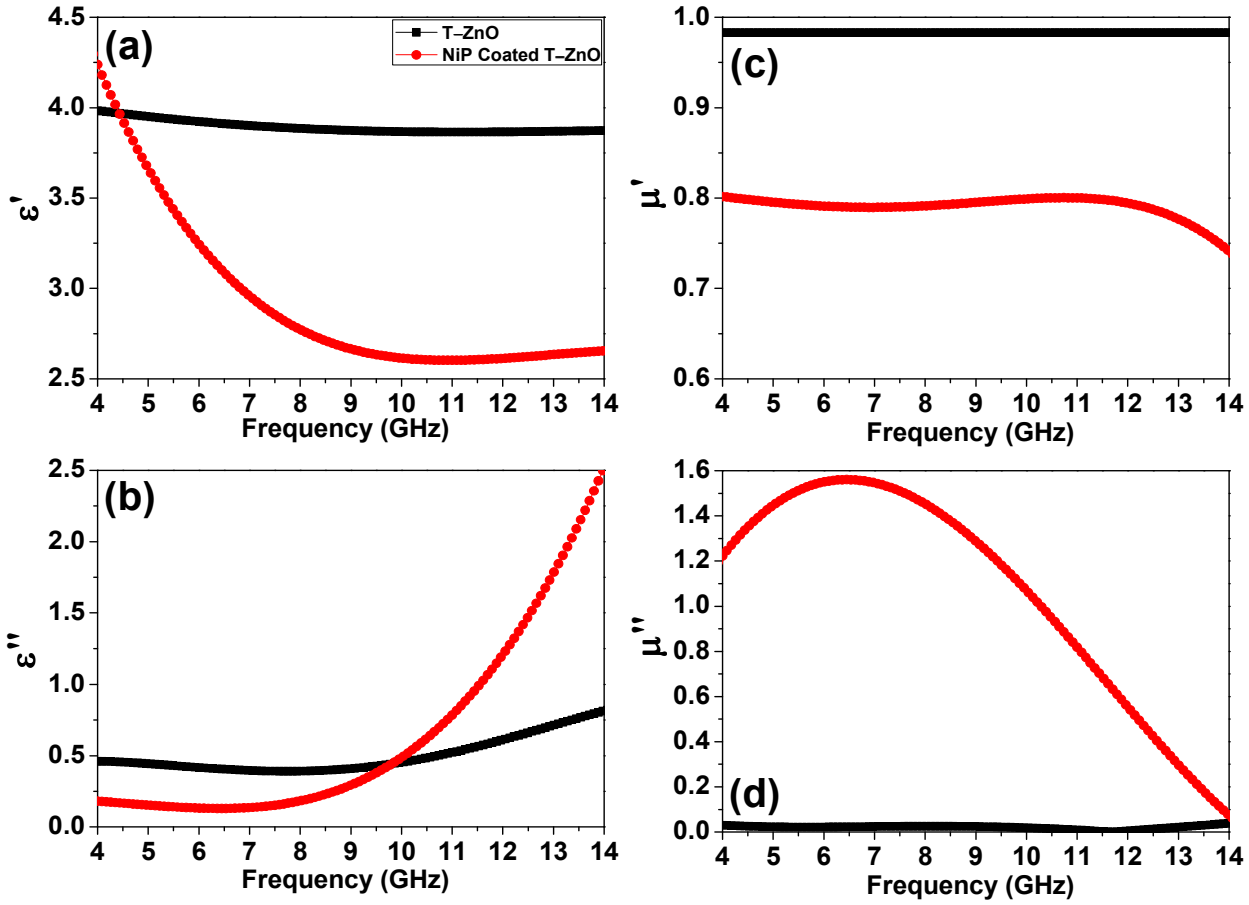

Figure 6. (a-d) The complex permittivity and permeability curves of "as-fabricated" T-ZnO and Ni-P coated T-ZnO nano-microstructures (black curve for as deposited ZnO tetrapods and red curve for NiP coated ZnO tetrapods).

Figure 7

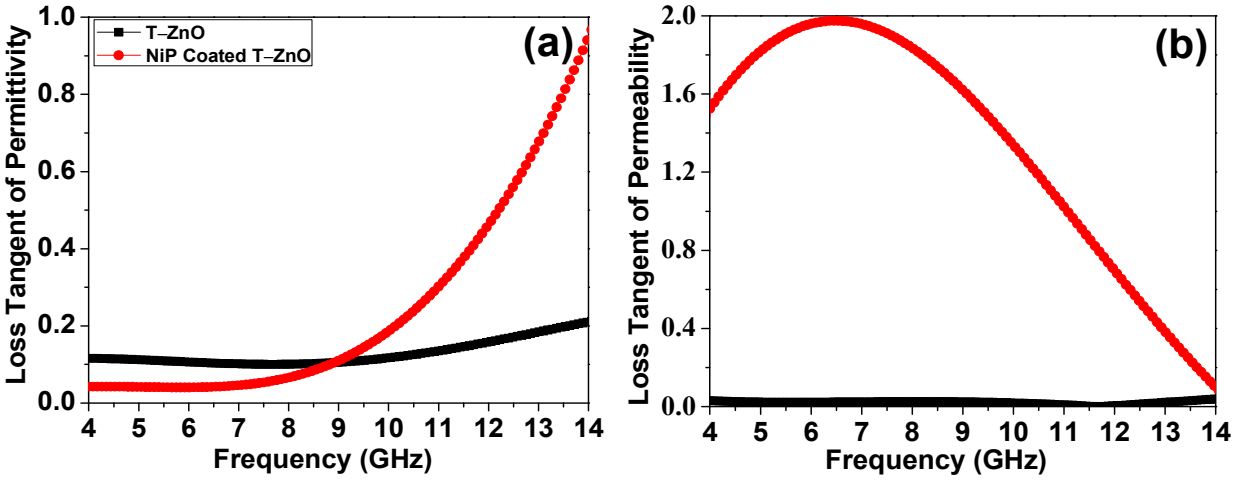

Figure 7. The loss tangents of "as-fabricated" T-ZnO and Ni-P coated T-ZnO nano-microstructures. (a) Dielectric loss tangents showing that dielectric losses are dominating at higher frequencies (> 10 GHz) for Ni-P coated T-ZnO and (b) magnetic loss tangents depicting that magnetic losses are dominating at lower frequencies (< 10 GHz) for Ni-P coated T-ZnO (black curve for as deposited ZnO tetrapods and red curve for NiP coated ZnO tetrapods).

Figure 8

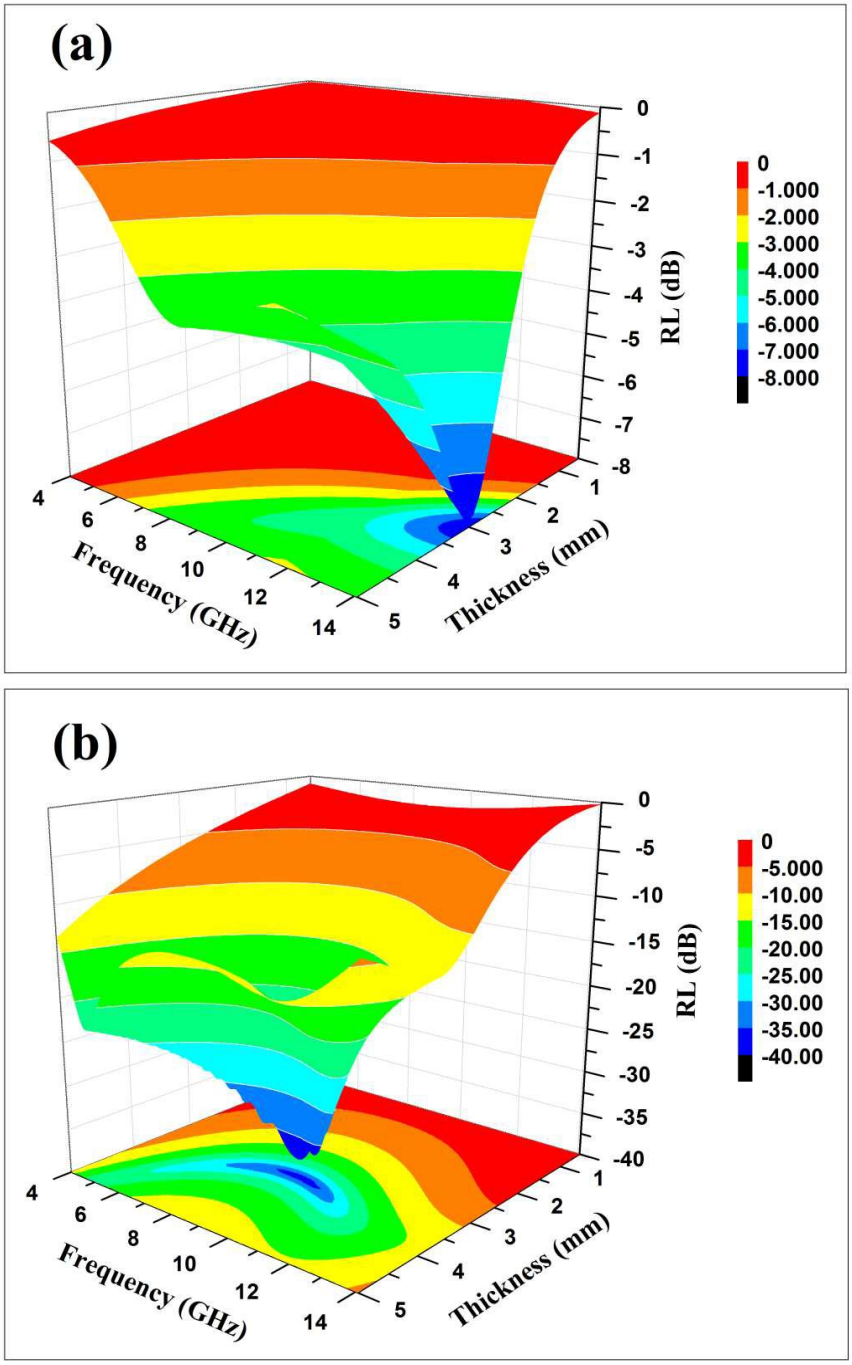

Figure 8. Frequency and thickness dependence of RL for (a) "as-fabricated" T-ZnO and (b) Ni-P coated T-ZnO samples. It can be seen that an absorber thickness of 2.6 mm and 3.4 mm for T-ZnO and Ni-P coated T-ZnO, respectively provides the best combination of bandwidth and RL value.

Figure 9

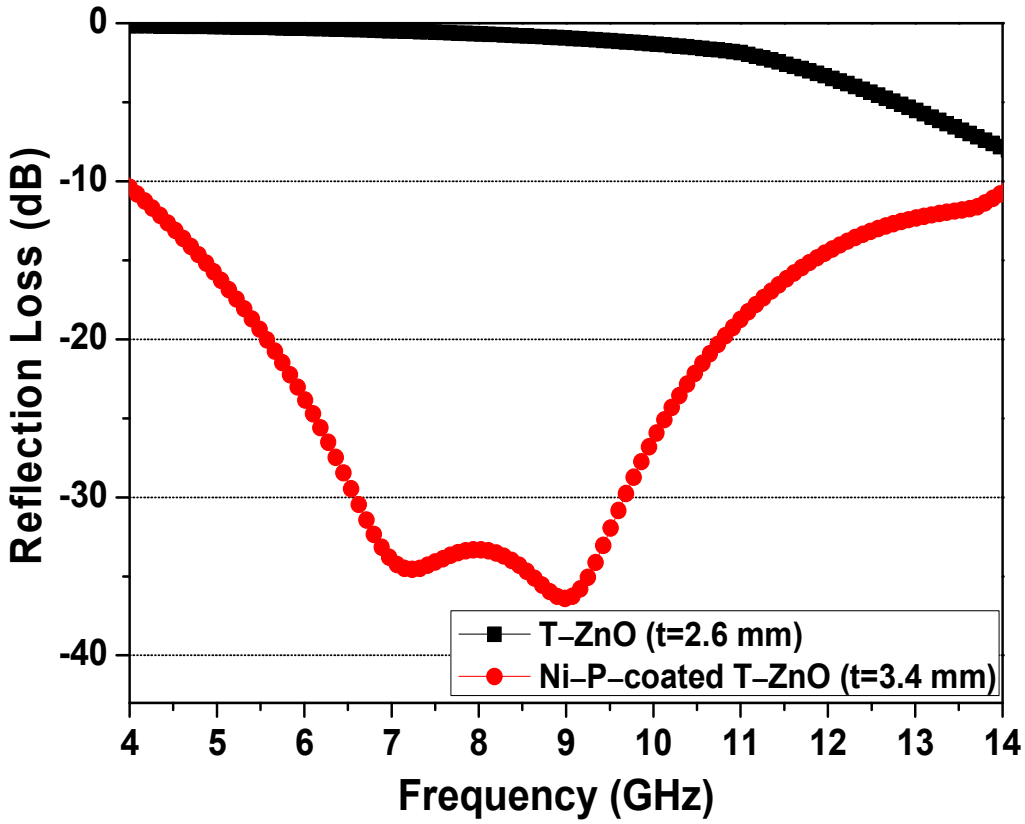

Figure 9. The RL curves of "as-fabricated" T-ZnO and Ni-P coated T-ZnO nano-microstructures at their respective optimum absorber thickness.

Table 1. Details of RL value along with their corresponding thickness and bandwidth for T-ZnO and Ni-P coated T-ZnO.

Sample	Peak *f* (GHz)	*d* (mm)	RL peak value (dB)	Bandwidth (GHz)		
				RL<-10	RL<-20	RL<-30
T-ZnO	14.0	2.6	-7.87	-	-	-
Ni-P-coated T-ZnO	8.99	3.4	-36.41	10.0 (4.0-14.0)	5.23 (5.57-10.80)	3.10 (6.57-9.67)

Graphical Abstract (TOC)

Tetrapod-shaped ZnO structures with high crystalline nature were synthesized by the simple flame transport synthesis approach and have been coated with Ni-P using the electroless deposition process for the realization of an efficient microwave absorbing composite material. Ni-P coated T-ZnO exhibited excellent microwave absorption properties having a peak RL value of −36.41 dB at 8.99 GHz and an ultra-wide bandwidth of 10.0 GHz (4.0-14.0 GHz) at RL< −10 dB and an absorber thickness of 3.4 mm.

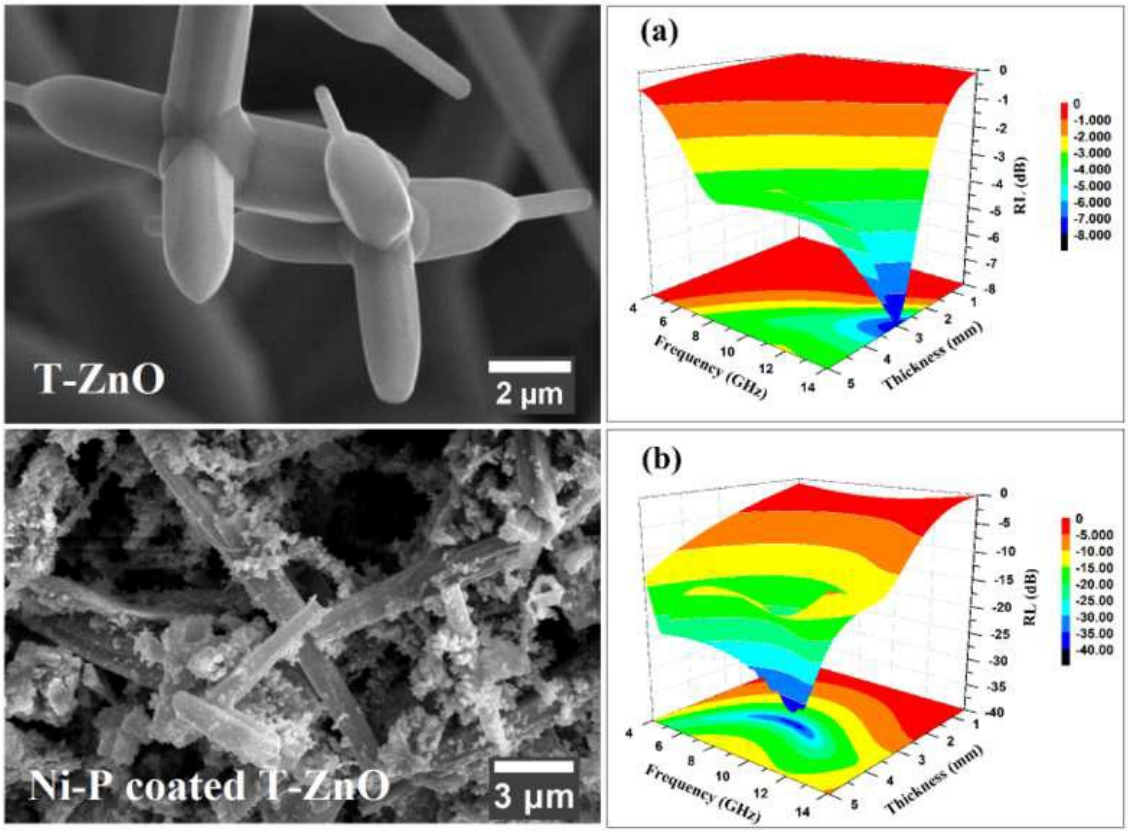

Supporting information

Figure S1. Image depicting the variation in color of powders of (a) "as-fabricated" T-ZnO (white), (b) pretreated T-ZnO after sensitization and activation (yellowish-brown), and (c) Ni-P coated T-ZnO (grayish-black).